Pergamon

Geochimica et Cosmochimica Acta, Vol. 68, No. 2, pp. 285–292, 2004

0016-7037/04 $30.00 + .00

doi:10.1016/j.gca.2003.07.001

Dissolution rates of pure methane hydrate and carbon-dioxide hydrate in undersaturated seawater at 1000-m depth

GREGOR REHDER,[1,*] STEPHEN H. KIRBY,[2] WILLIAM B. DURHAM,[3] LAURA A. STERN,[2] EDWARD T. PELTZER,[1] JOHN PINKSTON,[2] and PETER G. BREWER

[1]Monterey Bay Aquarium Research Institute, 7700 Sandholdt Road, Moss Landing, CA 95039-0628, USA
[2]U.S. Geological Survey, 345 Middlefield Road, Menlo Park, CA 94025, USA
[3]Lawrence Livermore National Laboratory, Livermore, CA 94550, USA

(*Received October* 6, 2002; *accepted in revised form July* 24, 2003)

Abstract—To help constrain models involving the chemical stability and lifetime of gas clathrate hydrates exposed at the seafloor, dissolution rates of pure methane and carbon-dioxide hydrates were measured directly on the seafloor within the nominal pressure-temperature (P/T) range of the gas hydrate stability zone. Other natural boundary conditions included variable flow velocity and undersaturation of seawater with respect to the hydrate-forming species. Four cylindrical test specimens of pure, polycrystalline CH_4 and CO_2 hydrate were grown and fully compacted in the laboratory, then transferred by pressure vessel to the seafloor (1028 m depth), exposed to the deep ocean environment, and monitored for 27 hours using time-lapse and HDTV cameras. Video analysis showed diameter reductions at rates between 0.94 and 1.20 μm/s and between 9.0 and $10.6 \cdot 10^{-2}$ μm/s for the CO_2 and CH_4 hydrates, respectively, corresponding to dissolution rates of 4.15 ± 0.5 mmol CO_2/m^2s and 0.37 ± 0.03 mmol CH_4/m^2s. The ratio of the dissolution rates fits a diffusive boundary layer model that incorporates relative gas solubilities appropriate to the field site, which implies that the kinetics of the dissolution of both hydrates is diffusion-controlled. The observed dissolution of several mm (CH_4) or tens of mm (CO_2) of hydrate from the sample surfaces per day has major implications for estimating the longevity of natural gas hydrate outcrops as well as for the possible roles of CO_2 hydrates in marine carbon sequestration strategies.

1. INTRODUCTION

A variety of low molecular weight liquids and gases are known to form a nonstoichiometric solid phase with water at cold temperatures and high pressures, known as gas hydrates (Sloan, 1998). Gas hydrates are currently a focus of research in applications that include the inhibition of plugged gas pipelines, the exploration of fossil fuels, and potential strategies of sequestering man-made CO_2. Much scientific work has focused on the nucleation, growth, and dissociation of gas hydrates, as well as on the prevention of hydrate formation by adding chemical inhibitors (Sloan, 1998). In contrast, the dissolution of hydrates has been largely neglected. These processes—in terms of thermodynamics—address the phase stability of gas hydrates and how gas hydrates respond to disequilibrium with other phases. Equilibrium requires the equality of temperature (T), pressure (P), and chemical potential (μ) in all phases. In the case of dissociation, gas hydrate generally becomes unstable by changing the P/T conditions in a way that the hydrate phase is not stable anymore, i.e., that the chemical potential of the gas component is lower in the free gas phase than in the hydrate phase (Fig. 1). If free water exists and the P/T conditions are within the hydrate stability field, then the chemical potentials of the gas component in the dissolved phase and the hydrate phase must be in equilibrium. Thus, the water has to be saturated with respect to the hydrate phase for the hydrate to remain stable.

The concentration of methane or carbon dioxide within the ocean is usually considerably smaller than its solubility (i.e., the concentration at equilibrium with the gas- or hydrate phases, respectively). Thus, for a hydrate exposed to ocean water, the hydrate phase and the water phase are typically not in equilibrium. Contact of hydrates with seawater or pore waters that are undersaturated in the hydrate-forming gas must cause hydrates to dissolve, but the rates of dissolution have not been established by measurements in the laboratory or in natural settings. The dissolution rates of gas hydrates that occur naturally on Earth therefore remain poorly constrained.

Natural gas hydrates, the most common being methane hydrate, are widely distributed in sediments along continental margins and are believed to harbor more hydrocarbon energy than contained in all other exploitable fossil fuel reservoirs (Kvenvolden, 1998). Massive gas hydrates have been reported as exposures on the seafloor in the Gulf of Mexico (MacDonald et al., 1994), and have also been found as accumulations in the upper sediment layer of Hydrate Ridge, off the coast of Oregon (Suess et al., 2001; Brewer et al., 2002). More recently, over 1000 kg of gas hydrate were recovered by a fishing trawler off Vancouver Island, in what may be the largest recovery ever reported from a marine setting (Spence and Chapman, 2001).

Pure CO_2 hydrates rarely occur in natural settings (Kvenvolden, 2000), and have so far been reported only from a single hydrogen sulfide-rich environment in the Okinawa Trough (Sakai et al., 1990). However, ocean disposal of fossil fuel CO_2 is now being actively considered as a means for sequestering CO_2 and mitigating climate change (Haugan and Drange, 1992; Kajishima et al., 1997). Several possible sequestration scenarios involving CO_2 hydrates have been considered. The success of liquid CO_2 release and storage in selected areas within ocean

* Author to whom correspondence should be addressed, at GEOMAR Research Center, Wischhofstr. 1-3, D-24148 Kiel, Germany (grehder@geomar.de).

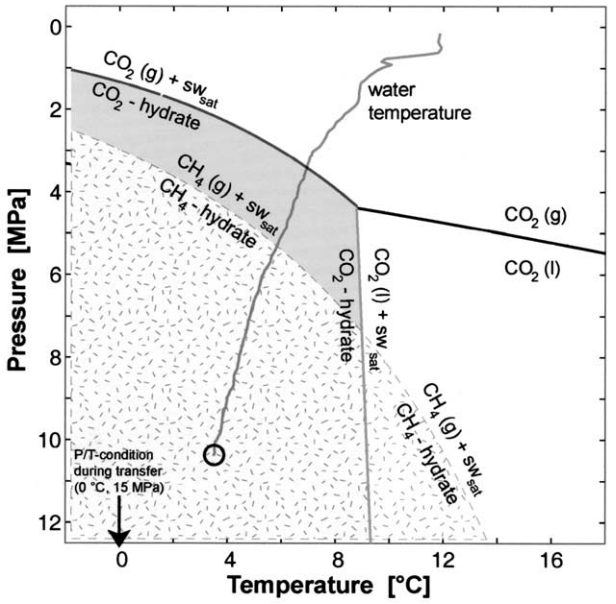

Fig. 1. P/T phase boundaries for the seawater-methane and seawater-carbon dioxide systems, respectively. Note that the phase diagram assumes that the seawater phase is saturated with CH_4 or CO_2, respectively. Also given is the profile of temperature versus pressure in Monterey Bay recorded on the first day of the experiment (February 1, 2001). The black circle indicates the P/T conditions during the experiment, the black arrow points towards the P/T conditions inside the pressure vessel within the ice-filled front drawer of ROV *Ventana* (15.5 MPa, 0°C) during transit to the seafloor.

basins might depend on the chemical stability of CO_2 hydrate formed at the CO_2-seawater interface.

Recent investigations of liquid CO_2 droplets covered by a hydrate skin in lab and field experiments have shown that the CO_2 hydrate rapidly dissolves in seawater (Shindo et al., 1995; Hirai et al., 1996; Hirai et al., 1997; Brewer et al., 2002), but quantitative measurements on the pure CO_2 hydrate phase are lacking. The CO_2 density within this structure-I hydrate, having a H_2O/CO_2 molar ratio of ~6:1, is considerably smaller than in liquid CO_2. Natural concentrations of CO_2 in sea water, mostly existing in the form of its ionic species HCO_3^-, are typically ≅2 mM, rendering the ocean very strongly undersaturated with respect to CO_2. Thus the concentrations and chemical potentials of CO_2 in all three phases are different under seafloor conditions and hence are in disequilibrium when they coexist.

Here we report on precise measurements of the dissolution rate of well-characterized, laboratory-synthesized methane and carbon-dioxide hydrates in an open-ocean seafloor setting and within the nominal pressure-temperature (P/T) range of the respective gas hydrate stability zones (Fig. 1). These experiments were carried out in situ to maintain essential boundary conditions such as undersaturation and flow velocity to emulate the exposure of natural gas hydrates and introduced CO_2 hydrate at the seafloor. These data are essential for predicting the lifetime of hydrates exposed on the sea floor, and thus for understanding the role of methane hydrates in climate change, and for fossil fuel CO_2 ocean sequestration studies.

2. EXPERIMENTAL

Cylindrical specimens of pure, polycrystalline CH_4 and CO_2 hydrate were grown in the laboratory by combining either cold, pressurized methane gas (27–32 MPa), or pressurized liquid carbon dioxide (17–25 MPa) with sieved granular water ice (~200 μm grain size) packed in stainless steel reaction vessels (Stern et al., 1996; Stern et al., 2000). Heating the reactants through the H_2O melting point and up to temperatures approaching the respective hydrate dissociation curves promotes complete reaction to gas hydrate. The resulting specimens have reproducible grain and pore characteristics and well-defined compositions of $CH_4 \cdot 5.89\ (\pm 0.01)H_2O$ and $CO_2 \cdot 5.75H_2O$, respectively (Stern et al., 1996; Stern et al., 2000; Circone et al., 2001; Circone et al., 2003). Following synthesis, the samples were slowly cooled to temperatures below −83°C and depressurized, then quenched to −196°C in liquid nitrogen for storage and transport. The CO_2 hydrates were flushed with CH_4 gas before quenching to prevent freezing of the CO_2 pore gas as a solid-CO_2 contaminant. No dissociation of the CO_2 hydrate occurred during this procedure, and exchange between CH_4 and CO_2 during this process is negligible (Circone et al., 2003). Previous lab experiments (Circone et al., 2003) also showed that CO_2 hydrate could be temporarily stabilized (for at least 48 h) under CH_4 pressure without any significant dissociation or CH_4 exchange, an important finding that facilitated the combined transport of CH_4 and CO_2 hydrate samples to the seafloor in one pressure vessel (see below). All samples for the dissolution experiment were then compacted hydrostatically to near-zero porosity by methods discussed previously (Stern et al., 1996; Stern et al., 2000), with resulting cylindrical shapes and dimensions of ~2.2 cm in diameter by 3 cm in length.

At −196°C, two samples each of fully dense methane and carbon-dioxide hydrate were placed within a custom-made rack that compartmentalized each sample in a vertical orientation. A flat polycarbonate front window permitted clear imaging. The semicircular backing of the rack was made from a flexible fine-mesh screen that permitted seawater flow around the samples. The sample rack was attached to the end cap of a 100-MPa stainless steel transport pressure vessel (Autoclave Engineering) with O-ring seals and a pin-closure mechanism, and outfitted with a pressure gage and a ball valve for venting gas.

The vessel was then quickly flushed and pressurized with methane, packed into a large ice bath for transport to the R/V *Point Lobos*, and loaded into an ice-filled front drawer of the ROV (remotely operated vehicle) *Ventana*. This ice pack arrangement for the pressure vessel provided stable conditions (0°C, 15.5 MPa) for the hydrates during their ROV-transit through the water column, and particularly through the warm near-surface ocean (temperature near 12°C; Fig. 1). Under the pressure conditions inside the vessel, CO_2 hydrate remains stable up to ~10°C, and CH_4 hydrate up to ~16°C. The pressure in the vessel was specifically chosen to be greater than that of the dive site, to ensure gas expulsion out of the vessel, rather than seawater infiltration into the vessel, during pressure equilibration at the seafloor.

The dive site was located in the subsurface Monterey Canyon in Monterey Bay, approximately 15 km off the coast of central California. Upon arrival at the seafloor at 1028 m water depth (10.48 MPa and 3.5°C), the packing ice floated away

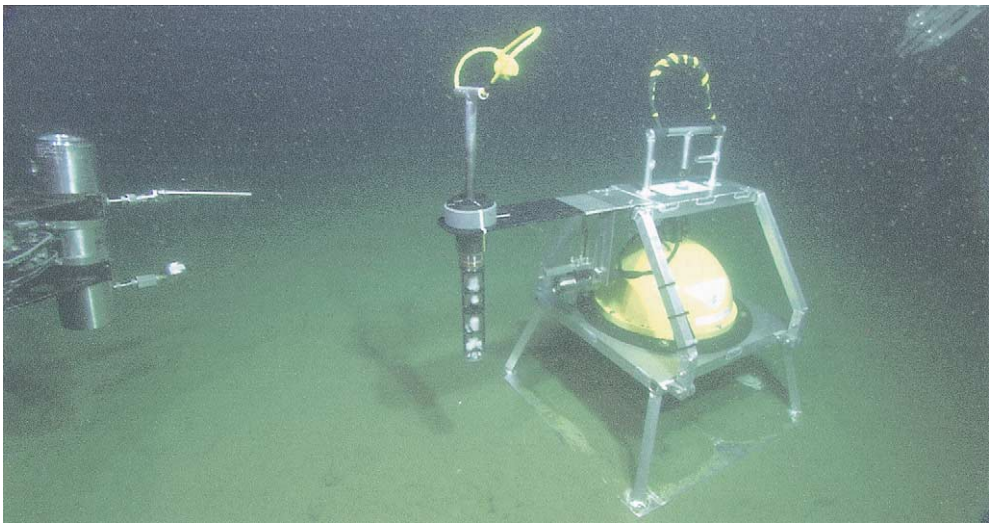

Fig. 2. Experimental apparatus on the seafloor as recorded by the HDTV video camera on the ROV *Ventana*. At the right is the time-lapse camera system with the sample rack containing the four hydrate samples. At the left is the open pressure vessel with release valve and differential pressure gage, secured by one of the ROV's two robotic arms. The other arm is just visible at the upper right.

after opening the front drawer of the ROV. The pressure vessel was then removed from the drawer by the robotic arm. Using a second arm, excess gas pressure was vented, the closure pin removed, and the end-cap with the attached sample rack was extracted from the vessel. The remaining trapped free gas and small crystals of newly formed methane hydrate were released during this step and rose out of the field of view of the ROV cameras. The rack was then placed in a sample stand attached to the custom-made aluminum frame of an AUVR 6000A autonomous underwater video system (Sound Ocean Systems Inc.) featuring a time-programmable Sony GV-A500 Hi8-video recorder (Fig. 2). Camera and sample stand had been preset for optimal illumination/resolution of the four hydrate samples. The samples were initially monitored for 2 h:19 min using *Ventana*'s on-board HDTV camera system (1920 × 1040 pixel resolution). The rack was then rotated 90°, so that the polycarbonate window faced the Hi8 camera. The autonomous Hi8 camera system then monitored the samples overnight in a time-lapse mode for 20 h:45 min (15 s recording every 15 min). After the R/V *Point Lobos* returned to the site on the next day, an additional 3 h:19 min of HDTV recording ended the video documentation before the equipment was recovered. Single frames were extracted from the HDTV and Hi8 video footage using Viewgraphics Clipper (HDTV) and Silicon Graphics Media Recorder software (Hi8) respectively, and standard image processing software was used for postprocessing and size measurements of the samples. We measured the widths of the samples relative to reference distances on the sample rack (Fig. 3), and derived the shrinking rates of the hydrates from the measurement of the change of the projected diameter of the individual samples over time. The dissolution rates were calculated from the diameter shrinkage rate using the equation:

$$DR = SR/2 * \rho_{Hyd}/M_G * (M_G/(M_G + HN * 0.018)) \quad (1)$$

where DR = Dissolution rate [mmol/m^2 s]; SR = Diameter shrinking rate [mm/s]—see text; ρ_{Hyd} = Density of hydrate [kg/m^3] = 1143 for CO_2, (based on linear extrapolation of thermal expansion data reported in Circone et al., 2003) and 923 for CH_4 (Stern et al., 1996; Stern et al., 2000); M_G = molar weight of the gas [kg/mol]; HN = hydrate number = 5.75 for CO_2 (Circone et al., 2003) and 5.89 for CH_4 (Stern et al., 1996; Stern et al., 2000).

3. RESULTS

Analysis of the time-lapse camera video showed that both CO_2 hydrate samples were completely dissolved after 3 h:55 min. Therefore, only the HDTV images of the first dive day were used to determine the dissolution rate of the CO_2 hydrate. During the first 2 h:19 min, the diameter of the two CO_2 hydrates decreased from 22 mm to 15 and 13 mm, respectively (Figs. 3a,b). Both CO_2 hydrates floated upwards for the last 30 min of their lifetime, possibly due to loss of CO_2 leaving a partially empty water cage structure.

The CH_4 hydrates dissolved more slowly (Figs. 3a,b and 3e,f). During the full 26.3 h experiment the upper (fixed) CH_4 hydrate shrunk from 20 to 11 mm in diameter (Figs. 3c,d). The lower (floating) CH_4 hydrate turned to a stable horizontal position during the rotation of the sample rack towards the time-lapse camera, and the change of the sample lengths was measured from Hi8-footage, showing a total decrease from 27 to 19 mm (Figs. 3c,d).

3.1. Carbon-Dioxide Hydrate Dissolution

The diameter reduction of the two CO_2 hydrates followed a generally linear trend with slopes of 0.94 (upper sample) and 1.20 μm/s (lower sample) (Fig. 4a), corresponding to dissolution rates of 3.6(2) and 4.6(7) mmol CO_2/m^{2}s. The slower rate of the upper sample may be the result of the observed tilting of the specimen one hour into the experiment, such that the surface of the sample was no longer orthogonal to the (horizontal) water motion, leading to lower exchange at the surface.

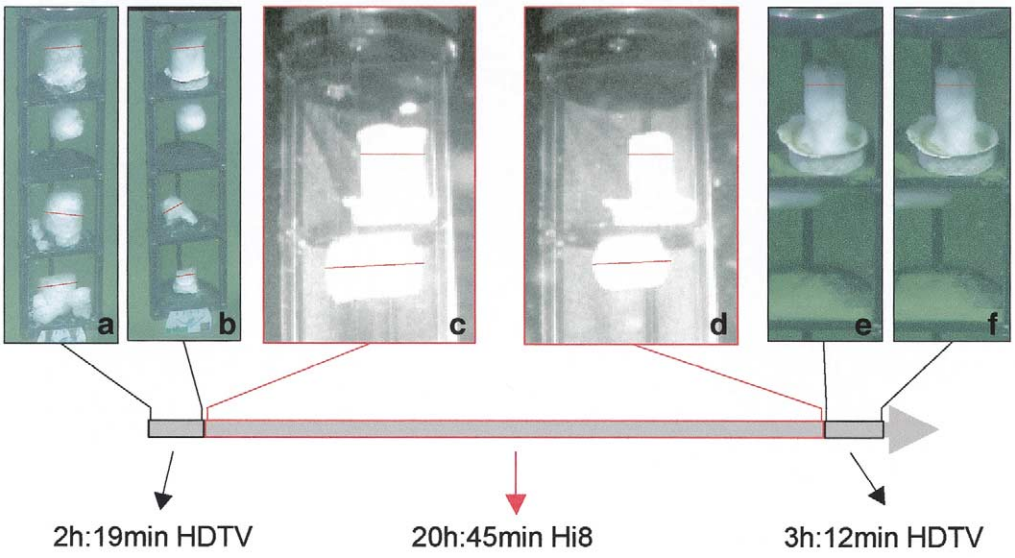

Fig. 3. Overview of the evolution of the samples over the duration of the experiment. Methane hydrates are in the upper two compartments, and carbon-dioxide hydrates in the lower two. Frames are from the beginning and end of the first phase of HDTV observation (a-b), from time-lapse camera observation (c-d), and from the final HDTV observation (e-f). Only the CH_4 hydrate samples are shown in (c-f). The CO_2 hydrate samples are completely dissolved shortly after frame (c). Thin red lines indicate width measurements of the samples. Note that the CO_2 hydrates stand on the bottom of the compartments, as their density (1.143 g/cm^3) is higher than the density of seawater. The CH_4 hydrates float because their density (0.923 g/cm^3) is less than that of seawater. The upper CH_4 hydrate specimen remains on the bottom of the compartment due to the weight of a metal jacket that remained attached at its base.

Small, correlated short-term oscillations about the general linear trend were observed for both samples, likely in response to changes in bottom current velocity. Qualitative assessment of the current velocity was possible from the imaged observation of marine particles in the seawater. Velocities were variable during the experiment, and periods of faster dissolution rates coincide with increased current velocity.

3.2. Methane Hydrate Dissolution

The methane hydrate samples dissolved about an order of magnitude more slowly than the carbon-dioxide hydrates did. Data collected during the first hour of HDTV observation were excluded because small pieces of methane hydrate formed in situ, and some small hydrate-covered gas bubbles were attached to the sample (see "clouded" appearance of the upper sample in Fig. 3a and clear view in Fig. 3b). These became detached during a period of high current velocity, and hence subsequent data were utilized. Data from the HDTV and Hi8 observation are in excellent agreement (Fig. 4b). The shrinking rate (diameter) for the upper hydrate sample, using the two different camera systems, was between 9.0 and 9.7 $\cdot$ 10^{-2} μm/s. In comparison, the shrinkage rate of the length of the lower methane hydrate sample, derived only from the time-lapse camera data, was 10.6 $\cdot$ 10^{-2} μm/s (Fig. 4c). The corresponding dissolution rates ranged from 0.34–0.4 mmol CH_4/m^{2}s. The lower resolution of the time-lapse camera in connection with the slower dissolution of the CH_4 hydrate made it impossible to observe short term deviations from the linear shrinking behavior as a result of changing current velocity.

4. INTERPRETATION

The ratio of the dissolution rates of the CO_2 to CH_4 hydrates is ~11, and can be readily explained using a diffusive boundary layer model. We assume that the dissolution of the hydrate is limited by diffusion of the dissolved gas into the bulk ocean, rather than by the kinetics of a chemical reaction at the hydrate surface, i.e., that dissolution is mass-transfer limited rather than reaction-limited. For this case, the dissolution rate can be formulated as the flux through a diffusive boundary layer:

$$F = D/Z * (c_s - c_w) \quad (2)$$

where D is the molecular diffusion coefficient in water of the guest species, Z is the thickness of the diffusive boundary layer, c_s is the gas concentration immediately at the phase boundary given by equilibrium with the solid (i.e., saturated), and c_w is the background concentration at some distance outside the diffusive boundary layer where the dissolved gas concentration is assumed to be uniform (Opdyke et al., 1987). The thickness of the diffusive boundary layer will depend mainly on physical parameters such as friction (i.e., water velocity), sample geometry, and water viscosity, (Santschi et al., 1991). However, given their proximity, we can assume that Z is identical for all four samples. The diffusion coefficients D of methane and carbon dioxide in water differ by less than 1% at the temperature of the experiment (Fig. 5; Jähne et al., 1987; Wanninkhof, 1992). The background concentrations of dissolved CH_4 and CO_2 in seawater are several orders of magnitude lower than the saturation concentration, so c_w can be neglected. Consequently, the ratio of the dissolution rates of CH_4 and CO_2 should be about equal to the ratios of their solubilities in seawater, thus:

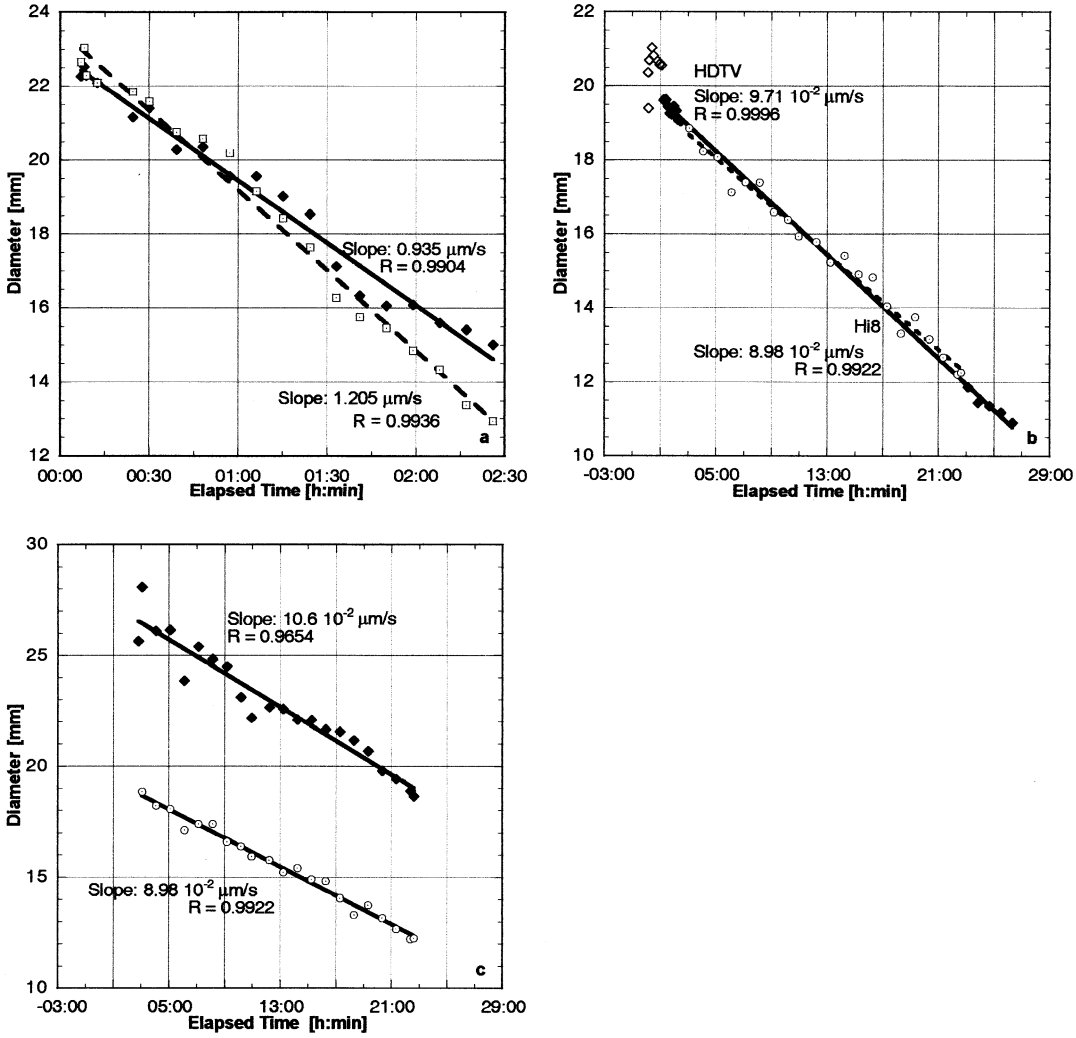

Fig. 4. (a) Diameter of the CO_2 hydrate samples versus time. Upper sample: black diamonds and solid line (linear fit): Lower sample: open squares and hatched line (linear fit). Note the correlated short-term oscillations about the general linear trend for both samples. (b) Diameter of the upper CH_4 hydrate sample versus time. Filled diamonds and solid line: measurements and linear fit using the HDTV observations at the beginning and the end of the experiment. Measurements of the first hour (open diamonds) were not included in the data analysis because in situ-formed CH_4 hydrate affected measurement accuracy. Circles and hatched line: measurements and linear fit using the Hi8 observations. (c) Comparison of the change in diameter of the upper CH_4 hydrate sample (open circles) with the change in length of the lower CH_4 hydrate sample (filled diamonds) versus time, as derived from the Hi8 observations.

$$F_{CH_4}/F_{CO_2} = C_{s(CH_4)}/C_{s(CO_2)} \quad (3)$$

The control of the solubility on the dissolution rate of CO_2 hydrate has already been demonstrated by Aya et al. (1997). We calculated the solubilities of methane and carbon dioxide in the presence of hydrates using the Multiflash software package (Infochem Ltd.), employing the Redlich-Kwong-Soave equation-of-state (Soave, 1972) for the fluid phases in combination with a standard thermodynamic model for gas hydrate systems (van der Waals and Platteeuw, 1959). We verified the model output against the available experimental data on CO_2 and CH_4 solubilities in water within the hydrate stability field (Aya et al., 1997; Kojima et al., 2002; Seo and Lee, 2002) as well as against other model calculations (Handa, 1990) for the case of CH_4; the experimental data are matched within 5%. The model emulates the observed trend of an increase in solubility with increasing temperature within the hydrate stability field, and a decrease in solubility with increasing temperature outside of the hydrate stability region (Aya et al., 1997; Kojima et al., 2002; Seo and Lee, 2002) (Figs. 6a,b). The recently published experimental data on CH_4 solubility (Seo and Lee, 2002) indicate a more pronounced pressure-dependence of the solubility than the thermodynamic models predict (Fig. 6b), but data and model results match very well for the in situ conditions of our experiment.

For the conditions of the experiment (P_{abs} = 10.48 MPa, T = 3.6°C, Salinity = 34.6), we calculate the solubility of CO_2 and CH_4 to be 0.728 mol/L and 0.0698 mol/L, respectively. The solubility ratio is 10.4. The solubility-controlled boundary-

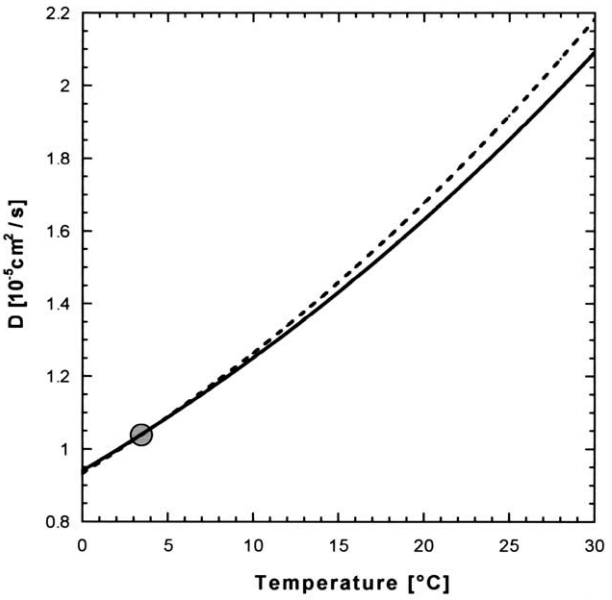

Fig. 5. Diffusion coefficients of methane (solid line) and carbon dioxide (hatched line) in pure water as a function of temperature (Jähne et al., 1987). The diffusion coefficients in seawater are ~6% lower (Jähne et al., 1987). Grey filled circle indicates the T-conditions at the dive site.

layer model predicts that the ratio of the dissolution rates should be the same as the solubility ratio, in good agreement with the measured ratio of 11. This finding strongly supports the initial assumption that the kinetics of the dissolution of both hydrates is diffusion-controlled.

Although the use of a single component (the hydrate forming gas) diffusion-controlled boundary layer model excellently matches the observations, and has been used for a theoretical prediction of gas hydrate dissolution before (Egorov et al., 1999), the approach has some shortcomings. The use of the diffusion coefficients of carbon dioxide and seawater measured by Jähne et al. (1987) neglects the presence of water clusters near the hydrate boundary, as inferred from nucleation theory. A change in the solvent structure is likely to affect the diffusion coefficient of the gas molecules. Also, a chemical potential gradient across the interface exists not only for the hydrate forming gas, but also for the water molecules. A detailed thermodynamic model of the dissolution of hydrates has been developed by Kvamme and coworkers (Kvamme and Tanaka, 1995; Kvamme, 2000; Kvamme and Kuznetsova, 2003). However, the diffusive boundary layer model is a reasonable first-order approach for the problem of mass-transfer controlled solid-phase dissolution in turbulent ocean conditions (Opdyke et al., 1987; Santschi et al., 1991; Egorov et al., 1999).

Within their corresponding hydrate stability fields, the solubilities of both CH_4 and CO_2 are expected to increase with temperature and to decrease with pressure (Kojima et al., 2002; Seo and Lee, 2002) (Figs. 6a,b), contrary to the expected trends outside the hydrate field. Therefore, the solubilities of both gases will decrease with depth within the ocean once the nominal hydrate phase boundary has been crossed. However, since the temperature in the ocean between 1000 m and abyssal depths decreases by only ~3–4°C, and the isothermal decrease in solubility with pressure is less than 3%/1000 m, the solubilities of both gases, as well as the hydrate dissolution rate, should not decrease by more than a factor of 2 between 1000 and 6000 m water depths (Fig. 6c). This is supported by experimental data on CO_2 hydrate dissolution rates and solubility (Aya et al., 1997). The decrease in solubility with increasing water depth for both gases below 1000 m is mainly caused by decreasing temperature. The effect of pressure on solubility within the hydrate stability field is small.

5. SIGNIFICANCE/CONCLUSIONS

The results of this work may not be directly applicable to the question of disposal of liquid CO_2 at the seafloor, which requires depths greater than ~2700 m, where liquid CO_2 becomes more dense than seawater (Brewer et al., 1999). For this case, 3 phases (aqueous, liquid CO_2, and hydrate) will be present. The liquid CO_2 will be unstable relative to formation of hydrate with water, while the hydrate (and the liquid CO_2) would be prone to dissolution due to the low CO_2 solute concentration (and thus low chemical potential) in the ambient seawater. In addition, a hydrate layer growing on the interface between water and liquid CO_2 will be gravitationally unstable because the density of CO_2 hydrate is higher than that of liquid CO_2 at depths shallower than ~5500 m.

In situ experiments at 3600 m water depth (Brewer et al., 1999, 2000) show that two behaviors can occur in almost identical experimental setups: (1) quantitative conversion of liquid CO_2 to hydrate (with the hydrate layer sinking through the liquid CO_2, renewing the liquid CO_2-water interface), and (2) dissolution from the top of the surface of liquid CO_2 without a bulk formation of hydrate. However, the rapid dissolution rate of carbon-dioxide hydrate reported here implies that in the case of the disposal of liquid CO_2 on the sea floor, the potential to form hydrate will not significantly enhance the longevity of the released CO_2. The transformation of liquid CO_2 to hydrate on the seafloor is thus unlikely to shield bulk CO_2 from dissolution. The residence time of CO_2 disposed at the seafloor will thus be determined by the effects of density stratification of CO_2-rich seawater (a stabilization of the benthic boundary layer) and ocean ventilation, rather than by the lifetime of CO_2 hydrate.

Dissolution of several mm methane hydrate per day in undersaturated seawater implies that long-term survival of seafloor hydrate outcrops observed today must be sustained by supply of sufficient CH_4 to maintain boundary layer saturation or continuous hydrate regrowth, as has been suggested by Egorov et al. (1999). The disappearance of such outcrops on sites revisited over a time period of several months (MacDonald et al., 1994) could be explained simply by dissolution after the supply with new gas from beneath the sediment has ceased or fallen below some threshold, without positing changes in seafloor temperatures or detachment of buoyant solid hydrate structures. The dissolution rate of gas hydrate might also be a key parameter controlling the supply of methane to microbial methane-oxidizing communities (Boetius et al., 2000) in hydrate bearing sediments. Future experimental work will address the dissolution of structure-II hydrates, which are also found in natural marine environments, as well as

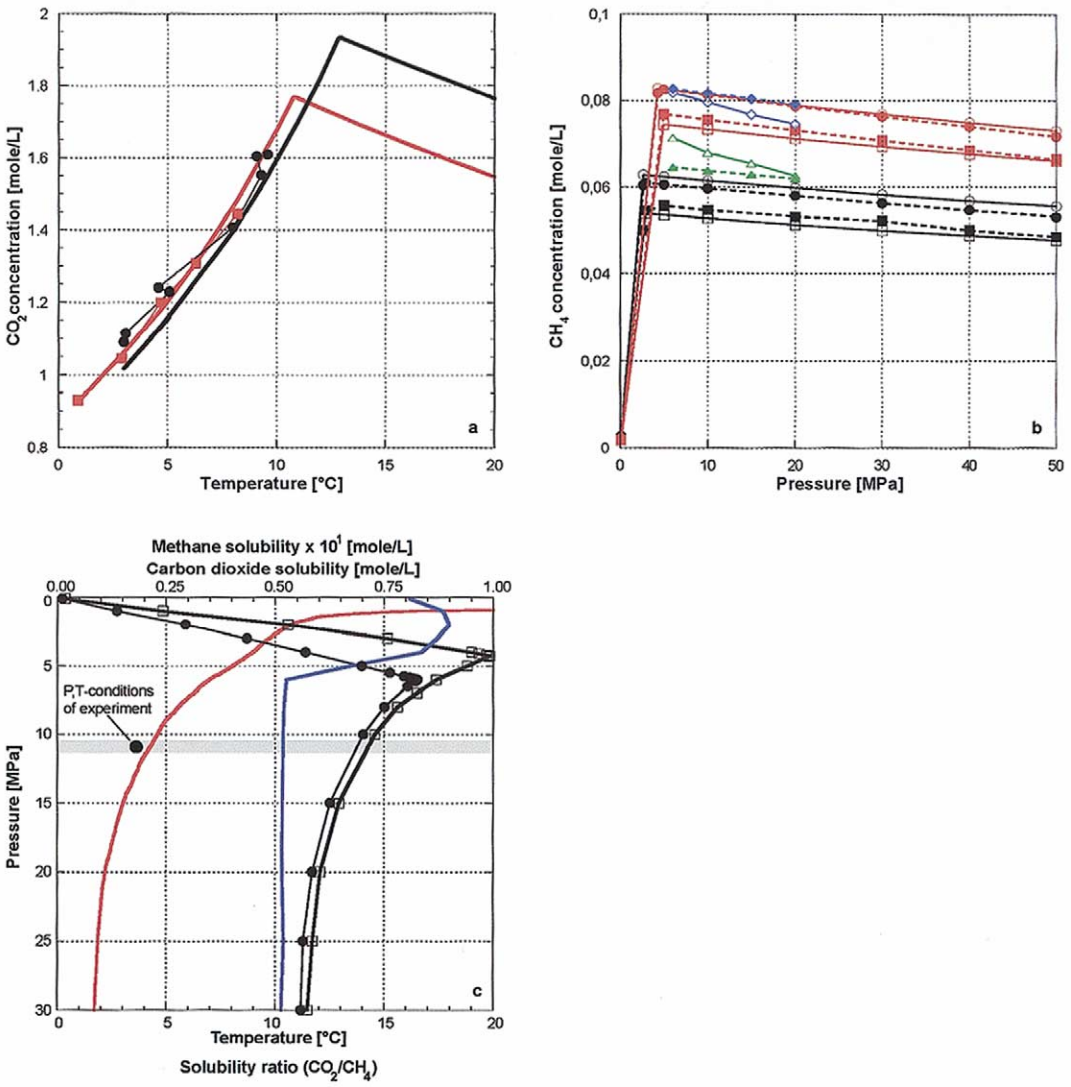

Fig. 6. (a) Temperature dependency of the solubility of CO_2 in water within and outside of the CO_2 hydrate stability field. Experimental data from Aya et al. (1997) (black points, 30 MPa) and Kojima et al. (2002) (red diamonds, 10 MPa) and trends predicted for 30 MPa (black line) and 10 MPa (red line) using Infochem Multiflash. (b) Pressure dependency of the solubility of CH_4 in water and seawater inside the CH_4 hydrate stability field. Black circles and open squares: trend predicted for 0°C for freshwater (circles) and for seawater with a salinity of 35 (squares) after Handa (1990); black dots and filled squares: same trends predicted using Infochem Multiflash. Red circles and open squares: trend predicted for 5°C for freshwater (circles) and for seawater with a salinity of 35 (squares) after Handa (1990); red dots and filled squares: same trends predicted using Infochem Multiflash; Open blue diamonds and open green triangles: experimental data for freshwater at 5°C (diamonds) and 1°C (triangles) (Seo and Lee, 2002); filled blue diamonds and green triangles: same trends predicted using Infochem Multiflash. (c) Estimated solubilities for CH_4 (black dots) and CO_2 (open black squares) between 0 and 3000 m water depth along a P/T profile in the equatorial North Pacific, using Infochem Multiflash. Also shown is the temperature profile (red) and the ratio of the solubilities (blue, CO_2/CH_4) which stays almost constant at a value of 10.4 within the region of hydrate stability for both gases. Black point and grey-shaded area indicate conditions similar to those during the experiment. For Figure 6a and b, the solubility in [mol/L] was calculated from the original data given as weight fractions (Aya et al., 1997; Kojima et al., 2002) or mole fractions (Handa, 1990; Seo and Lee, 2002), respectively.

the effects of hydrate porosity, hydrate-sediment mixtures, and sediment cover on hydrate dissolution.

We specifically targeted our study to measure dissolution on clean hydrate-seawater interfaces. Any process that isolates hydrates exposed on the seafloor from chemical reaction with seawater (such as hydrocarbon films, surfactants, or microbial layers) might significantly lower the dissolution rates reported here.

Acknowledgments—We thank the captain and the crew of R/V *Point Lobos* and the technicians and pilots of ROV *Ventana* for their skillful support during offshore operation. The help of Chris Rogers-Walz and Kyra Schlining in the video labs is gratefully acknowledged. We thank Susan Circone for her assistance in synthesizing the CO_2 hydrate samples The detailed reviews of Dr. Izuo Aya (Maritime Research Institute, Osaka), Dr. Bjørn Kvamme (University of Bergen), and an unknown reviewer were highly appreciated and helped to improve the manuscript. This work was supported by a grant to MBARI from the

David and Lucile Packard Foundation and funding from the U.S. Geological Survey Gas Hydrate Project and a contract from the Department of Energy under the Carbon Sequestration Program. Work performed by W. D. Durham under the auspices of the U.S. Department of Energy by the Lawrence Livermore National Laboratory under contract W-7405-ENG-48. This is publication no. GEOTECH-27 of the program GEOTECHNOLOGIEN of BMBF and DFG.

Associate editor: F. A. Podosek

REFERENCES

Aya I, Yamane K, and Nariai H. (1997) Solubility of CO_2 and density of CO_2 hydrate at 30 MPa. *Energy* **22,** 263–271.

Boetius A, Ravenschlag K, Schubert C, Rickert D, Widdel FGA, Amann R, Jorgensen BB, Witte U, and Pfannkuche O. (2000) A marine microbial consortium apparently mediating anaerobic oxidation of methane. *Nature* **407,** 623–626.

Brewer PG, Friedrich G, Peltzer ET, and Orr FM Jr. (1999) Direct experiments on the ocean disposal of fossil fuel CO_2. *Science* **284,** 943–945.

Brewer PG, Peltzer ET, Friederich G and Rehder G. (2000) Progress in direct experiments on the ocean disposal of fossil fuel CO_2 (abstract). *Eos Trans. Am. Geophys. Union* **81(Suppl),** B11D-07.

Brewer PG, Paull CK, Peltzer ET, Ussler W, Rehder G and Friederich G. (2002) Measurements of the fate of gas hydrates during transit through the ocean water column. *Geophys. Res. Lett*. **29,** DOI: 10.1029/2002GL014727.

Brewer PG, Peltzer ET, Friederich G, and Rehder G. (2002) Experimental determination of the fate of rising CO_2 droplets in seawater. *Environ. Sci. Techn.* **36,** 5441–5446.

Circone S, Kirby SH, Pinkston JC, and Stern L. (2001) Measurement of gas yields and flow rates using a custom flow meter. *Rev. Sci. Instruments* **72,** 2709–2716.

Circone S, Stern LA, Kirby SH, Durham WB, Chakoumakos BC, Rawn CJ, and Rondinone AJ. (2003) CO_2 hydrate: Synthesis, composition, dissociation behavior, and a comparison to structure I CH_4 hydrate. *J. Phys. Chem. B* **107,** 5529–5539.

Egorov AV, Crane K, Vogt PR, and Rozhkov AN. (1999) Gas hydrates that outcrop the sea floor: Stability models. *Geo-Marine Lett.* **19,** 68–75.

Handa YP. (1990) Effect of hydrostatic pressure and salinity on the stability of gas hydrates. *J. Phys. Chem.* **94,** 2652–2657.

Haugan PM and Drange H. (1992) Sequesteration of CO_2 in the deep ocean by shallow injection. *Nature* **357,** 318–320.

Hirai S, Okazaki K, Araki N, Yazawa H, Ito H, and Hijikata K. (1996) Transport phenomena of liquid CO_2 in pressurized water flow with clathrate-hydrate at the interface. *Energy Convers. Mgmt.* **37,** 1073–1078.

Hirai S, Okazaki K, Tabe Y, Hijikata K, and Mori Y. (1997) Dissolution rate of liquid CO_2 in pressurized water flows and the effect of clathrate films. *Energy* **22,** 285–293.

Jähne B, Henz G, and Dietrich W. (1987) Measurement of the diffusion coefficients of sparingly soluble gases in water. *J. Geophys. Res.* **92 (C10),** 10767–10776.

Kajishima T, Saito T, Nagaosa R, and Kosugi S. (1997) GLAD: A gas-lift method for CO_2 disposal into the ocean. *Energy* **22,** 257–262.

Kojima R, Yamane K, and Aya I. (2002) Dual nature of CO_2 solubility in hydrate forming regions. Presented at the 6th International Conference on Greenhouse Gas Control Technologies.

Kvamme B. (2000) Phase transitions and stabilities in seawater containing carbon dioxide. In *Recent Advances in Marine Science and Technology*, pp. 279–289. Honolulu, Hawaii USA, monograph.

Kvamme B and Tanaka H. (1995) Thermodynamic stability of hydrates for ethane, ethylene, and carbon dioxide. *J. Phys. Chem.* **99,** 7114–7119.

Kvamme B and Kuznetsova T. (in press) Hydrate dissociation in chemical potential gradients: Theory and simulations. *Fluid Phase Equilibria*.

Kvenvolden KA. (1998) A primer on the geological occurrence of gas hydrates. In *Gas Hydrates: Relevance to World Maring Stability and Climate Change* Vol. 137 (eds. JP Henriet and J Mienert), pp. 9–30. Geological Society.

Kvenvolden KA. (2000) Chap. 2. in *Natural Gas Hydrate in Oceanic and Permafrost Environments* (ed. M. D. Max), pp. 9–16. Kluwer.

MacDonald IR, Guinasso NL Jr, Sassen R, Brooks JM, Lee L, and Scott KT. (1994) Gas hydrate that breaches the sea floor on the continental slope of the Gulf of Mexico. *Geology* **22,** 699–702.

Opdyke BN, Gust G, and Ledwell JR. (1987) Mass transfer from smooth alabaster surfaces in turbulent flows. *Geophys. Res. Lett.* **14,** 1131–1134.

Sakai HY, Gamo E-S, Kim M, Tsutsumi T, Tanaka T, Ishibashi J, Wakita H, Yamano M, and Omori T. (1990) Venting of carbon dioxide-rich fluid and hydrate formation in mid-Okinawa Trough backarc basin. *Science* **248,** 1093–1096.

Santschi PH, Anderson RF, Fleisher MQ, and Bowler W. (1991) Measurements of diffusive sublayer thicknesses in the ocean by alabaster dissolution, and their implications for the measurements of benthic fluxes. *J. Geophys. Res.* **96,** 10641–10657.

Seo Y and Lee H. (2002) Hydration number and two-phase equilibria of CH_4 hydrate in the deep ocean sediments. *Geophys. Res. Lett*. **29,** 10.1029/2001GL014226.

Shindo Y, Hakuta T, Fujioka Y, Takeuchi K, and Komiyama H. (1995) Controlling effect of CO_2 hydrate membrane on CO_2 dissolution into water from the surface of liquid CO_2. *Energy Convers. Mgmt.* **36,** 479–484.

Sloan ED. (1998) *Clathrate Hydrates of Natural Gases*. Marcel Dekker.

Soave G. (1972) Equilibrium constants from a modified Redlich-Kwong equation of state. *Chem. Eng. Sci.* **27,** 1197–1203.

Spence GD. and Chapman NR. (2001) Fishing trawler nets massive "catch" of methane hydrates. *EOS Trans. Am. Geophys. Union* **82,** 621.

Stern LA, Kirby SH, and Durham WB. (1996) Peculiarities of methane clathrate hydrate formation and solid-state deformation, including possible superheating of water ice. *Science* **273,** 1843–1848.

Stern LA, Kirby SH, Durham WB, Circone S, and Waite WF. (2000) Synthesis of pure methane hydrate suitable for measurement of physical properties and decomposition behavior. In *Natural Gas Hydrate in Oceanic and Permafrost Environments* (ed. MD Max), pp. 323–349. Kluwer.

Suess E, Torres ME, Bohrmann G, Collier RW, Rickert D, Goldfinger C, Linke P, Heuser A, Sahling H, Heeschen K, Jung C, Nakamura K, Greinert J, Pfannkuche O, Trehu A, Klinkhammer G, Whiticar MJ, Eisenhauer A, Teichert B, and Elvert M. (2001) Sea floor methane hydrates at Hydrate Ridge, Oregon. In *Natural Gas Hydrates: Occurrence, Distribution, and Detection*, Vol. 124 (eds. CK Paull and WP Dillon), pp. 87–98. American Geophysical Union.

van der Waals JH and Platteeuw JC. (1959) Clathrate solutions. In *Advances in Chemical Physics*, Vol. 2 (ed. I. Prigogine), pp. 2–57. Interscience.

Wanninkhof R. (1992) Relationship between wind speed and gas exchange over the ocean. *J. Geophys. Res.* **97(C5),** 7373–7382.